RSC Advances

ROYAL SOCIETY OF CHEMISTRY

www.rsc.org/advances

Journal Name

RSCPublishing

ARTICLE

Butylamino-functionalized cellulose nanocrystal films: barrier properties and mechanical strength

Cite this: DOI: 10.1039/x0xx00000x

Miikka Visanko[a*], Henrikki Liimatainen[b], Juho Antti Sirviö[b], Kirsi S. Mikkonen[c], Maija Tenkanen[c], Rafal Sliz[d], Osmo Hormi[e], Jouko Niinimäki[b]

Received 00th January 2012,
Accepted 00th January 2012

DOI: 10.1039/x0xx00000x

www.rsc.org/

Cellulose nanocrystals (CNCs), which are strong, rod-like constituents of plant cellulose, are promising materials for green packaging applications as the material is capable of forming tortuous network structures with efficient barrier against outside gasses. Here, a two-step procedure based on periodate oxidation followed by reductive amination was used as a pretreatment to modify bleached birch chemical wood pulp. Individualized CNCs were obtained from three different butylamino-functionalized pulps by mechanical homogenization. The fabricated CNCs were utilized to form transparent barrier films with a vacuum filtration method. All the butylamino-functionalized CNC films showed capability to resist oxygen permeability even at high relative humidity (RH 80%), and values low as 5.9 ± 0.2 cc•µm/(m^2•d•kPa) were recorded for pure cellulose based film using tert-butylamino-functionalized CNCs. In addition barrier against water vapor permeation and dynamic vapor sorption was determined up to relative humidity of 80 and 90 %, respectively. For surface characterization of the films time-dependent contact angles and surface roughness were measured. The films had good mechanical characteristics with tensile strength of 105.7 ± 9.7 MPa, strain-to-failure of 6.4 ± 0.6 % and a Young's modulus of 5.8 ± 0.8 GPa.

Introduction

Fabrication of nanofibrillated cellulose (NFC) has been demonstrated in several studies where divergent chemical [1], mechanical [2], or enzymatic pretreatments [3] or combinations [4] of the preceding have been used to individualize nanofibrils with diameter of 3-4 nm and length of several micrometers. In addition, production of stiff and strong cellulose nanocrystals (CNCs) via acid hydrolysis [5,6] or lately by advanced chemical pretreatments [7,8] has been substantiated. Both NFC and CNCs have many superior properties compared to corresponding macro scale materials: high specific surface area, lightweight, transparency and strength of individual nanocellulosic particulates make them an attractive choice for use in various reinforcing or protecting layer structures.

Prospective use of these nano-scale celluloses in promising future bioproducts has been the endeavor of many scientists to introduce competitive renewable materials that can replace the current petrochemical based products. The growing amount of plastic packaging waste being produced worldwide could ideally be replaced with biodegradable alternatives such as cellulose. The use of cellulose in barrier layer structures has been studied for this purpose, as the high level of crystallinity [9] and the dense network structure formed by the nano-sized cellulose particulates could help protect the material against gasses and vapor [10]. Native cellulose has a hydroxyl group-rich surface, making it hydrophilic: thus, it is difficult for it to create a sufficient barrier against moist conditions. This issue has been addressed with different post-surface modifications [11], cross-linkers [12], covalent coupling [13], or coatings [14] to create efficient moisture resistance.

The use of pure CNCs or NFCs as well as their hybrids with nano-sized mineral particles has resulted in advanced film materials with favorable properties such as fire retardancy [15,16], high strength [4,17], lightweight, flexibility [18,19], and controlled porosity [20]. Resistance against, grease [21], gas [17,22] and water vapor [23] have also been attained. Specifically, the combination of NFC with mineral particles has been shown to result in excellent barrier properties. Nacre-like layered structure [24] creates a tortuous path inside the NFC network where gasses can hardly pass, as the minerals act as impermeable void-sealing constituents. Barrier properties are especially desired in food packaging applications, as strict regulations call for the use of materials, that can dispense sufficient protection against outside gasses, light, and other impurities [25]. Simultaneously, rising petroleum cost and increasing consumer demands for naturally occurring recyclable raw materials for packaging has

increased the pressure to find new cost-effective materials [26]. In addition to sufficient barrier properties, high strength and flexibility are also expected in electronic devices such as organic solar cells [27] and organic light emitting diodes (OLED) [28].

So far, research efforts on nanocellulosic films have focused on NFC-based materials [29], whereas the properties of CNC based films [30] have been far less addressed. Here, our aim was for the first time demonstrate fabrication of self-standing barrier films from amphiphilic butylamino-functionalized CNCs and to address their barrier performance. The major fraction of the film consisted of individualized CNCs, which were produced through acid free treatment [31]. Their suitability to perform as an effective barrier layer against oxygen and water vapor permeability in elevated humidity levels was examined. Dynamic vapor sorption (DVS), mechanical strength, surface roughness, and time-dependent contact angles were also measured.

Experimental

Materials

Bleached birch (*Betula pendula*) chemical wood pulp was used as a cellulosic raw material to fabricate CNCs using consequent periodate oxidation and reductive amination. $NaIO_4$ (India, purity ≥ 99.0%) and LiCl (Germany, ≥ 98.0%) for fabrication of dialdehyde cellulose (DAC) were obtained from Sigma-Aldrich. For the reductive amination of dialdehyde cellulose, 2-picoline borane (Sigma-Aldrich, USA (95%)) and three butylamine isomers, isobutylamine hydrochloride (Tokyo Chemical Industry, Belgium >99%), *n*-butylamine hydrochloride (Tokyo Chemical Industry, Belgium >98%), and *tert*-butylamine hydrochloride (Sigma-Aldrich, Switzerland ≥ 98.0%), were purchased. These chemicals were used as received without any further purification. Ethanol (96%) to wash butylamino-modified pulp was bought from VWR (Finland).

Fabrication of butylamino-functionalized CNC films

Acid-free pretreatment of cellulose fibers was used for fabrication of butylamino-functionalized CNCs for film structures using previously reported two-step procedure based on periodate oxidation followed by reductive amination [31]. In brief, the cellulose pulp was first converted to DAC with lithium chloride (LiCl) assisted sodium metaperiodate ($NaIO_4$) oxidation as previously reported [32]. Oxidation was conducted at 75 °C for 3 h to attain DAC with 3.79 mmol g^{-1} of aldehydes. Three separate CNC grades were fabricated via reductive amination of DAC with butylamine isomers. A 10-fold excess of iso-, *n*-, or *tert*-butylamine hydrochloride in relation to the aldehyde groups of DAC was mixed with deionized water (900 ml), and the pH of the solution was set to 4.5 with a dilute HCl. DAC fibers (9 g) and a 2-fold excess of 2-picoline borane, based on the assessed amount of the aldehyde groups, were added to the suspension, and the reaction was continued for 72 h under magnetic stirring in a closed container at room temperature. The reaction was stopped by removing the residual chemicals by filtration and the pulp was washed with ethanol and water. The chemically pretreated pulp was mechanically individualized to CNCs with a homogenizer (APV- 200, Denmark) with three bypasses (220, 480, 600 bar). The substituent content of CNCs after reductive amination based on elemental analysis was 0.567, 0.562 and 0.072 for iso-, *n*- and *tert*-butylamino, respectively. The lower reactivity with *tert*-butylamine was suspected to result from steric effects, as iso- and *n*-butylamine were sterically less demanding.

Self-standing films were manufactured from the butylamino-functionalized CNCs using a vacuum filtration method. First, 200 mg abs. from each butylamino suspension was diluted to 0.25% concentration by mixing with deionized water using the UltraTurrax mixer (IKA T25, Germany) at 10,000 rpm for 3 min. The mixed sample was degassed under pressurized vacuum suction in combination with gentle magnet stirring. Finally, the degassed suspension was carefully poured into a glass filter funnel (7.2 cm in diameter) covered in a polyvinylidene fluoride (PVDF) membrane (pore size 0.65 µm). In the beginning of filtration, a low pressure (5-10 kPa) was used to constitute an effective CNC network before increasing the pressure gradually up to 80 kPa. The purpose for the low vacuum pressure was to retain the CNCs without passing straight through the pores of the PVDF membrane. After filtration, a wet gel-like film was formed and was left to dry in a desiccator overnight. Prior to further analysis, the CNC-film was carefully peeled off from the PVDF membrane.

Optical transmittance of the self-standing films

Transmittance from the self-standing butylamino-functionalized films was measured with an UV-Vis-NIR spectrophotometer (Carry 500 Scan, Varian Inc., USA) near the visible light wavelength from 350 to 800 nm with a step size of 1 nm. In addition, the visual appearance of the butylamino-functionalized films was portrayed against a background image.

Surface roughness

The roughness measurements were performed using an optical profilometer (Bruker ContourGT, USA). A vertical scanning interferometry method, with a broadband (normally white) light source, was applied during measurements. The size of the inspected area was 0.3 mm^2 (0.634 x 0.475 mm) and was determined by optics used in the measurement setup. Morphological images were taken in three different locations for each sample, and average (R_a) and root square (R_q) roughnesses were extracted. Consequently, obtained values of each sample were averaged and standard deviations calculated.

Oxygen permeability

The oxygen transmission rate (OTR) of the films was measured using an oxygen permeability (OP) analyser with a coulometric sensor (M8001; Systech Illinois, Oxfordshire, UK). The film was exposed to 100% oxygen on one side and to oxygen-free nitrogen on the other side. The OP was calculated by multiplying the OTR by the thickness of the film and dividing it by the oxygen gas partial pressure difference between the two sides of the film. The measurements were carried out at 23°C, normal atmospheric pressure, and relative humidities (RHs) of 50% and 80%. After measuring the performance in RH 50% the RH was raised to 80% and the measurement was continued for the same sample until equilibrium of the OTR was reached. The specimen area was 5 cm^2 and the thickness of the film was measured before analysis at four points with a micrometer at 1 µm precision. All the films were preconditioned in the same environment for at least one day prior to measurement (OTR, WVTR, tensile testing). The OP was determined in duplicate.

Water vapor permeability

The water vapor permeability (WVP) was determined, using an RH gradient of 0/52%. Films were sealed on aluminium cups containing 43 g $CaCl_2$ as a desiccant. There was an air gap of 6 mm between the salt and the underside of the film. The cups were placed in a desiccator cabinet equipped with a fan to circulate the air above the samples at a speed of 0.15 m/s. The cabinet was kept at 22°C and its RH was maintained at 52% using a saturated $Mg(NO_3)_2$ solution.

The cups were weighed five times over the course of five days. The temperature and RH of the cabinet were measured using a Rotronic RH meter (Bassersdorf, Switzerland) prior to each weighing. The water vapor transmission rate (WVTR) was calculated from the linear regression of the slope of weight gain vs. time by dividing the slope by the film area. The water vapor partial pressure at the underside of the film was calculated using the correction method [33]. The water vapor permeability (WVP) was obtained by multiplying the WVTR by the thickness of the film and dividing it by the water vapor partial pressure difference between the two sides of the film. Duplicates of each film type were tested and their thicknesses were measured prior to testing at 4 points at 1 µm precision.

Dynamic vapor sorption

A DVS Intrinsic sorption microbalance (Surface Measurement Systems, Alperton, Middlesex, UK) was used to collect water sorption isotherms of the films. The experiments were carried out in duplicate at 25 °C and RH values from 0 to 90%. The sample was hydrated stepwise in 10% RH steps by equilibrating the sample weight at each step. The moisture uptake was calculated according to Equation (1):

$$Moisture\ uptake = 100 * \frac{W_{moist} - W_{dry}}{W_{dry}}, \qquad (1)$$

where W_{moist} is the sample weight equilibrated at the chosen RH and W_{dry} is the weight of the dry sample.

Contact angle measurement

Time-dependent contact angles were measured from the fabricated films by applying a static sessile-drop contact-angle measurement. The measurements were carried out with a Krüss DSA100 (Germany) system. The instrument was equipped with a high-speed camera (360 fps) and analysis software. The contact angle was determined immediately after the drop (< 2µl) formed on the film surface and the time-dependent contact angles were determined every 60 seconds for a time-period of ten minutes. Contact angles were extracted with the height-width method, in which a rectangle enclosed by a contour line was regarded as the segment of a circle. As a result, contact angles were calculated from the height-width relationship of the enclosing rectangle. For each sample, three droplets in different locations were studied, the results were averaged, and the standard deviations were calculated.

Mechanical properties

The tensile tests were performed with a universal material testing machine (Instron 5544, USA) equipped with a 100 N load cell. The butylamino-functionalized films were cut into thin strips with a specimen width of 5 mm and a thickness of ~ 34 µm. For the tensile testing a 40 mm gauge length was set under a strain rate of 4 mm/min where six specimens were measured in total. The thickness of each specimen was measured with a Lorentzen & Wettre micrometer at 1µm precision (Sweden) from three different locations in between the gauge length and the results were averaged. The tests were conducted in relative humidity of 50% at a temperature of 23 ˚C and under a prestrain of 0.05–0.1 N. The Young's modulus was calculated from the initial linear part of the stress-strain curve, and the ultimate tensile strength was defined as the stress at specimen breakage. Bulk density for the films was determined by oven drying a 30 x 30 mm square piece from each specimen at 105 °C. The dried films were weight and average dimension were measured to calculate the densities.

Results and discussion

Physical properties of the butylamino-functionalized CNCs

The pretreatment of cellulose fibers with periodate oxidation followed by reductive amination and homogenization resulted in homogenous nanocrystal suspensions. The advantage of using the current pretreatment eases the preparation of CNCs as the washing of the reactive chemicals is straightforward, and complicated separation processes such as dialysis against distilled water or centrifugation are not required. Also the targeted surface functionalities can be introduced before the crystallinities are liberated and no additional post-treatments are required. In depth characterization of the CNCs has been

reported previously [31]. In summary, the morphology of the butylamino-functionalized CNCs after mechanical homogenization was similar with each specimen with a typical width of 3-4 nm and length of 150-200 nm based on the transmission electron microscope image analysis (Fig. 1). All the CNCs occurred individually without aggregation. The crystallinity of the CNCs was ~55% according to wide-angle x-ray diffraction measurements and no change to other crystalline form from cellulose I was observed. Based on the similar morphology and x-ray diffraction patterns the results indicated the physical properties of the CNCs did not dependent on the used butylamine isomer used. However, the fabrication of CNCs without the reductive amination reaction step was shown not to be possible. Consequently, we were not able to fabricate reference material without the butylamine functionalization.

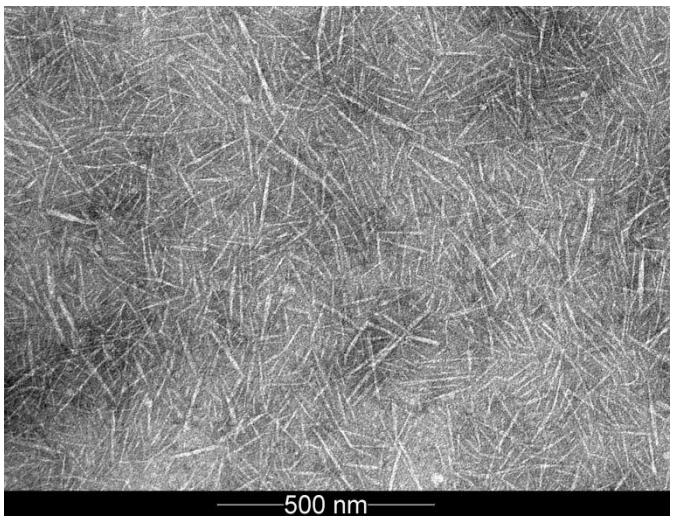

Fig. 1 TEM-image of individually occurring CNCs from isobutylamino-functionalized suspension.

Optical and surface properties of the fabricated films

Optically transparent self-standing films were obtained from all the butylamino-functionalized CNCs after drying and removal of the PVDF membrane (Fig. 2). Majority of the CNCs remained on top of the PVDF membrane without passing through as the yield was approximately 85-90% after vacuum filtration. When the films were placed against a background image, the printed text was seen sharply although the transmittance of the films was below 30%. The films had lower transmittances than previously reported for NFC based films [22]. However, both the film thickness and chosen fabrication method influence the optical properties of CNC films.

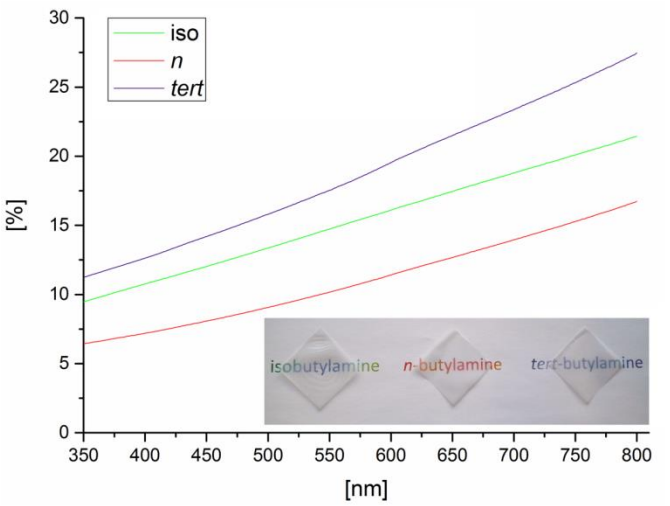

Fig.2 Appearance of self-standing films from butylamino-functionalized CNCs and optical transmittance in the visual light wavelengths.

All the films exhibited rather smooth surfaces as illustrated in Figure 3. Of the samples, the film from *tert*-butylamino had the most uneven surface structure; this could be attributed to remaining larger particles such as microfibril bundles, which is also suggested by our previous results [31]. Here we did not use a fractionation method to separate larger particles from the CNC suspensions. These larger particles can probably be separated from individual CNCs using centrifugation as previously shown [34]. However, the fabrication method based on vacuum filtration on top of a microporous PVDF membrane partly affects the formation of an uneven surface. The pressure from the vacuum creates a fingerprint mark from both the glass filter funnel and the PVDF membrane to the surface of CNC film. Thin films from pure CNCs have been reported to have a surface roughness (R_q) of 2.3 nm based on atomic force microscopy (AFM) measurements [35,36] when spin coating or casting on a smooth glass were applied. Thus an alternative fabrication method would undoubtedly reduce the surface roughness and improve the transmittance of the films.

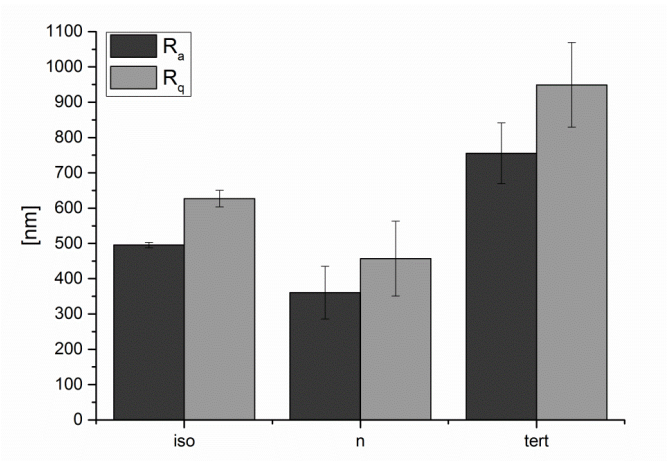

Fig. 3 Surface roughness of the top layer for films fabricated from butylamino-functionalized CNCs. Error bars represent standard deviation of three measurements.

The surface characteristics of self-standing butylamino-functionalized CNC films were studied by measuring time-dependent water contact angles under the constant presence of a water droplet. As the films were not fully impermeable, the droplet started to infiltrate and spread on the films' surfaces, which can be seen in descending contact angles against time (Fig. 4). Isobutylamino-functionalized CNC film showed highest hydrophobicity due to higher substituent content as stated earlier [8]. The small increase in contact angle during the first minute with *n*- and *tert*-butylamino-functionalized films was caused by initial swelling of the film surface, after which the values started to decline. This behaviour was not observed with isobutylamino-functionalized CNC film. The descending rate during the measured time period was slowest for *tert*-butylamino-functionalized film. Crystalline cellulose should not swell in water, but according to the results water is absorbed inside the butylamino-functionalized CNC films. Absorption of water has also been reported previously with other CNC films [9]. Sorption of water and film swelling was assumed to occur in small pore cavities, which are located between the crystals [37].

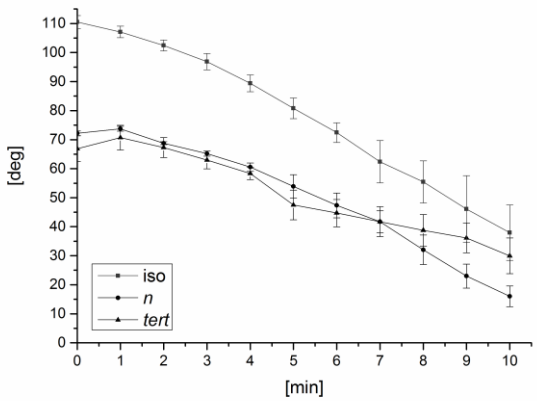

Fig. 4 Time-dependent water contact angles for butylamino-functionalized CNC films. Error bars represent standard deviations of three measurements.

Barrier against oxygen

At a high RH of 80%, the OTR of *tert*-butylamino-functionalized CNC film remained at a relatively low level (Table 1). Previously OTR, has been reported to increase exponentially at high RHs with both pure NFC and hybrid films [22,38]. At an RH of 80%, iso- and *n*-butylamino-functionalized CNC films had twice as high of an OTR compared to that of *tert*-butylamino-functionalized CNC film. This effect is likely related to structural differences between the films, which might be linked to the degree of hydrogen bonding within the film network. Previously, reduced hydrogen bonding caused by cellulose hydrophobization has been shown to impair the barrier properties of NFC films [39]. Here, the reactivity and the amount of substitution with *tert*-butylamine were much lower than with iso- or *n*-butylamine [31]. Therefore, it is likely that the level of hydrogen bonding with the film of *tert*-butylamino-functionalized CNCs was higher, as there were fewer alkyl groups attached to the cellulose backbone. The higher level of hydrogen bonding reduced the occurrence of nano-sized cavities in the film and thus resulted in a more compact structure that presented more resistance to gas molecules. Moreover, the conformational differences between butylamino-functionalized CNCs may have affected the packing of CNCs and permeability of films

All the films possessed low OP, values indicating their good barrier potential toward oxygen (Table 1). Especially, OP at elevated RHs was very low for *tert*-butylamino-functionalized film. At RH 50% the values for *tert*-butylamino-functionalized films were similar than reported earlier for periodate oxidation-based α-hydroxy sulfonic acid cellulose nanofibrils (0.2 cc•µm/(m^2•d•kPa) [40], TEMPO oxidized cellulose nanofibrils (TOCNs) (0.2 cc•µm/(m^2•d•kPa) [17], mechanically fabricated MFC (0.2 cc•µm/(m^2•d•kPa) [41], enzymatically modified NFC (0.26 cc•µm/(m^2•d•kPa) [42] and lower than films manufactured from carboxymethylated NFC (0.85, 0.52 cc•µm/(m^2•d•kPa) [22,43]. In our previous study, values twice as low in the same environment were reported when dicarboxylic acid cellulose (DCC) nanofibrils were utilized for film formation [40]. The oxygen permeability of nanocellulosic films is typically significantly increased at elevated RH [22,39,42], but for the tert-butylamino-functionalized CNC film, low oxygen permeability was maintained even at an RH of 80%. Recently, films fabricated from cellulose nanofibrils that were partly converted to dialcohol cellulose attained similar values (5.5 ± 0.8 cc•µm/(m^2•d•kPa) [19]. However, these films were mechanically pressed during drying, which aids the formation of denser structure and thus reduces the OP.

Barrier against water vapor and DVS

The WVP according to the measurements of the butylamino-functionalized films was similar with each other and no significant differences in the results were noted (Table 2). According to the DVS measurement, all the films steadily adsorbed water up to 60% RH (Fig. 5), after which the adsorption increased more rapidly as a function of RH. Compared to iso- and *n*-butylamino-functionalized CNC films, the *tert*-butylamino-functionalized film had a slightly lower tendency for moisture adsorption at the higher RH.

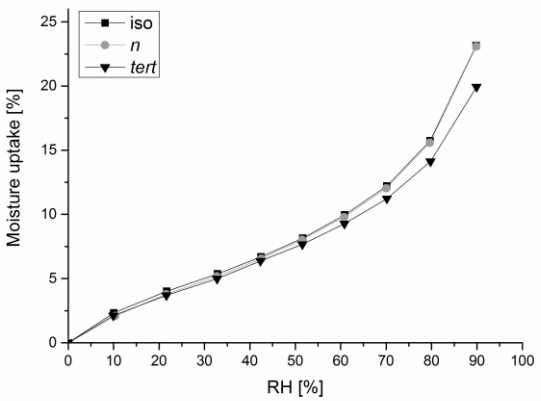

Fig. 5 Dynamic vapor sorption for butylamino-functionalized CNC films in RH 0-90%.

Mechanical strength of the films

Tensile testing of the butylamino-functionalized CNC films revealed how the films' mechanical properties (Table 3) were affected by the hydrophobic modification. Presumably, the attachment of alkyl groups to the CNCs' surfaces reduces the

Table 1. Oxygen transmission rate (OTR) and oxygen permeability (OP) of films (mean ± standard deviations from duplicate measurements).

Sample:	OTR ± sd [cc/(m^2·d)]		OP ± sd [cc·µm/(m^2·d·kPa)]	
	(RH 50%)	(RH 80%)	(RH 50%)	(RH 80%)
isobutylamino	2.3 ± 0.2	39 ± 5	0.78 ± 0.02	13 ± 0.8
n-butylamino	2.4 ± 0.02	41 ± 3	0.79 ± 0.01	14 ± 0.6
tert-butylamino	0.76 ± 0.2	18 ± 1	0.25 ± 0.07	5.9 ± 0.2

Table 2. Water vapor transmission rate (WVTR) and water vapor permeability (WVP) of films (mean ± standard deviations from duplicate measurements).

Sample:	WVTR ± sd [g/(m^2·d)] (RH 0/52%)	WVP ± sd [g·mm/(m^2·d·kPa)] (RH 0/52%)
isobutylamino	103 ± 2	2.8 ± 0.1
n-butylamino	123 ± 0.9	3.3 ± 0.1
tert-butylamino	136 ± 35	3.3 ± 0.9

Table 3. Mechanical properties (RH 50%) and density of the butylamino-functionalized CNC films, where standard deviation is based on six measurements.

Sample:	Tensile strength [MPa]	Young's modulus [GPa]	Strain at break [%]	Bulk density [kg/m^3]
Iso	96.0 ± 8.0	5.7 ± 0.3	5.6 ± 0.4	1420
n	105.7 ± 9.7	5.8 ± 0.8	6.4 ± 0.6	1410
tert	113.7 ± 4.9	6.3 ± 0.6	3.4 ± 0.2	1400

hydrogen bonding between CNCs and thus results in higher strain at break for iso- and *n*-butylamine. Fewer hydrogen bonds between CNCs allow greater slippage within the network and thus increase the strain before film breakage. The lower strain at break, the slightly higher tensile strength, and Young's modulus with *tert*-butylamino-functionalized film with minor alkyl group content support these findings. Overall, the lack of longer and more flexible filaments in the network structure affects the properties of the butylamino-functionalized films, as higher tensile strengths are commonly seen when cellulose nanofibrils have been utilized for film fabrication [44]. The bulk densities for oven-dried butylamino-functionalized CNC films indicated the formation of compact structure as the density for cellulose nanocrystal has been reported to be 1600 kg/m^3 [45].

Conclusions

Butylamino-functionalized CNC films were tested for their suitability for divergent packaging applications based on their barrier properties and strength. The study found that, overall, *tert*-butylamino-functionalized films had the best barrier resistance against oxygen and vapor sorption. Introduction of hydrophobic alkyl groups was seen to increase the oxygen permeability and reduce the tensile strength of the films, as the hydrogen bonding between the CNCs was believed to decrease when the alkyl group content rises. As *tert*-butylamino-functionalized CNCs had the least amount of alkyl groups attached, it was hypothesized that they would form a more compact structure with greater barrier resistance, in contrast to iso- or *n*-butylamino. Valuable results were reported showing how the use of neat CNCs can produce environmentally friendly barrier films that can compete with current petrochemical-based products. In future studies, the fine properties of the butylamino-functionalized CNCs could be further advanced in other composite and barrier applications in which improved qualities can be attained by embedding the CNCs to a supporting matrix structure or mixing them with additional fillers.

Acknowledgements

Financial support from the Thule Institute is acknowledged. The authors also acknowledge the support from the Future Biorefinery Programme of Finnish Bioeconomy Cluster, FIBIC Ltd. The facilities of the Center of Microscopy and Nanotechnology of the University of Oulu were utilized in this research. The Academy of Finland is acknowledged for funding KSM (project number 268144). We also thank Tanja Liukkonen and Suvi Alakalhunmaa for technical assistance in the OTR, WVTR and DVS analyses.

Notes and references

[a] Fibre and Particle Engineering Laboratory & Thule Institute, P.O. Box 4300, FI-90014 University of Oulu, Finland
[b] Fibre and Particle Engineering Laboratory, P.O. Box 4300, FI-90014 University of Oulu, Finland
[c] Department of Food and Environmental Sciences, P.O. Box 27, FI-00014 University of Helsinki, Finland
[d] Optoelectronics and measurement techniques laboratory, P.O Box 4500, FI-90014 University of Oulu, Finland
[e] Department of Chemistry, P.O. Box 3000, FI-90014 University of Oulu, Finland
*Corresponding author

References

1 H. Liimatainen, M. Visanko, J. A. Sirviö, O. E. O. Hormi and J. Niinimaki, *Biomacromolecules*, 2012, **13**, 1592–1597.
2 S. Iwamoto, A. N. Nakagaito and H. Yano, *Appl. Phys. A*, 2007, **89**, 461–466.
3 M. Henriksson, G. Henriksson, L. A. Berglund and T. Lindström, *Eur. Polym. J.*, 2007, **43**, 3434–3441.
4 H. Liimatainen, N. Ezekiel, R. Sliz, K. Ohenoja, J. A. Sirviö, L. Berglund, O. Hormi and J. Niinimäki, *ACS Appl. Mater. Interfaces*, 2013, **5**, 13412–13418.
5 M. Matos Ruiz, J. Y. Cavaille, A. Dufresne, J. F. Gerard and C. Graillat, *Compos. Interfaces*, 2000, **7**, 117–131.
6 M. N. Anglès and A. Dufresne, *Macromolecules*, 2001, **34**, 2921–2931.
7 A. C. W. Leung, S. Hrapovic, E. Lam, Y. Liu, K. B. Male, K. A. Mahmoud and J. H. T. Luong, *Small*, 2011, **7**, 302–305.

8 M. Visanko, H. Liimatainen, J. A. Sirviö, J. P. Heiskanen, J. Niinimäki and O. Hormi, *Biomacromolecules*, 2014, **15**, 2769–2775.
9 C. Aulin, S. Ahola, P. Josefsson, T. Nishino, Y. Hirose, M. Osterberg and L. Wågberg, *Langmuir ACS J. Surf. Colloids*, 2009, **25**, 7675–7685.
10 G. Chinga-Carrasco and K. Syverud, *Nanoscale Res. Lett.*, 2012, **7**, 1–6.
11 G. Rodionova, M. Lenes, Ø. Eriksen and Ø. Gregersen, *Cellulose*, 2011, **18**, 127–134.
12 Q. Yang, T. Saito and A. Isogai, *Cellulose*, 2012, **19**, 1913–1921.
13 A. Benkaddour, C. Journoux-Lapp, K. Jradi, S. Robert and C. Daneault, *J. Mater. Sci.*, 2014, **49**, 2832–2843.
14 P. Lu, H. Xiao, W. Zhang and G. Gong, *Carbohydr. Polym.*, 2014, **111**, 524–529.
15 A. Liu, A. Walther, O. Ikkala, L. Belova and L. A. Berglund, *Biomacromolecules*, 2011, **12**, 633–641.
16 A. Liu and L. A. Berglund, *Eur. Polym. J.*, 2013, **49**, 940–949.
17 C.-N. Wu, T. Saito, S. Fujisawa, H. Fukuzumi and A. Isogai, *Biomacromolecules*, 2012, **13**, 1927–1932.
18 P. A. Larsson, L. A. Berglund and L. Wågberg, *Cellulose*, 2014, **21**, 323–333.
19 P. A. Larsson, L. A. Berglund and L. Wågberg, *Biomacromolecules*, 2014, **15**, 2218–2223.
20 H. Sehaqui, Q. Zhou, O. Ikkala and L. A. Berglund, *Biomacromolecules*, 2011, **12**, 3638–3644.
21 J. A. Sirviö, A. Kolehmainen, H. Liimatainen, J. Niinimäki and O. E. O. Hormi, *Food Chem.*, 2014, **151**, 343–351.
22 C. Aulin, G. Salazar-Alvarez and T. Lindström, *Nanoscale*, 2012, **4**, 6622.
23 T. T. T. Ho, T. Zimmermann, S. Ohr and W. R. Caseri, *ACS Appl. Mater. Interfaces*, 2012, **4**, 4832–4840.
24 P. Podsiadlo, A. K. Kaushik, E. M. Arruda, A. M. Waas, B. S. Shim, J. Xu, H. Nandivada, B. G. Pumplin, J. Lahann, A. Ramamoorthy and N. A. Kotov, *Science*, 2007, **318**, 80–83.
25 T. V. Duncan, *J. Colloid Interface Sci.*, 2011, **363**, 1–24.
26 A. Khan, T. Huq, R. A. Khan, B. Riedl and M. Lacroix, *Crit. Rev. Food Sci. Nutr.*, 2014, **54**, 163–174.
27 L. Hu, G. Zheng, J. Yao, N. Liu, B. Weil, M. Eskilsson, E. Karabulut, Z. Ruan, S. Fan, J. T. Bloking, M. D. McGehee, L. Wågberg and Y. Cui, *Energy Environ. Sci.*, 2013, **6**, 513.
28 C. Charton, N. Schiller, M. Fahland, A. Holländer, A. Wedel and K. Noller, *Thin Solid Films*, 2006, **502**, 99–103.
29 M. Nogi, S. Iwamoto, A. N. Nakagaito and H. Yano, *Adv. Mater.*, 2009, **21**, 1595–1598.
30 H. Yang, A. Tejado, N. Alam, M. Antal and T. G. M. van de Ven, *Langmuir*, 2012, **28**, 7834–7842.
31 M. Visanko, H. Liimatainen, J. A. Sirviö, J. P. Heiskanen, J. Niinimäki and O. Hormi, *Biomacromolecules*, 2014, 140627102029009.
32 J. Sirvio, U. Hyvakko, H. Liimatainen, J. Niinimaki and O. Hormi, *Carbohydr. Polym.*, 2011, **83**, 1293–1297.
33 A. Gennadios, C. L. Weller and C. H. Gooding, *J. Food Eng.*, 1994, **21**, 395–409.
34 Y. Habibi, L. A. Lucia and O. J. Rojas, *Chem. Rev.*, 2010, **110**, 3479–3500.
35 C. D. Edgar and D. G. Gray, *Cellulose*, 2003, **10**, 299–306.
36 M. Eriksson, S. M. Notley and L. Wågberg, *Biomacromolecules*, 2007, **8**, 912–919.
37 T. A. Dankovich and D. G. Gray, *J. Adhes. Sci. Technol.*, 2011, **25**, 699–708.
38 A. Liu and L. A. Berglund, *Carbohydr. Polym.*, 2012, **87**, 53–60.
39 A. Lozhechnikova, D. Dax, J. Vartiainen, S. Willför, C. Xu and M. Österberg, *Carbohydr. Polym.*, 2014, **110**, 163–172.
40 J. A. Sirviö, A. Kolehmainen, M. Visanko, H. Liimatainen, J. Niinimäki and O. E. O. Hormi, *ACS Appl. Mater. Interfaces*, 2014, **6**, 14384–14390.
41 M. Österberg, J. Vartiainen, J. Lucenius, U. Hippi, J. Seppälä, R. Serimaa and J. Laine, *ACS Appl. Mater. Interfaces*, 2013, **5**, 4640–4647.
42 S. Galland, Y. Leterrier, T. Nardi, C. J. G. Plummer, J. A. E. Månson and L. A. Berglund, *J. Appl. Polym. Sci.*, 2014, **131**, n/a–n/a.
43 C. Aulin, M. Gällstedt and T. Lindström, *Cellulose*, 2010, **17**, 559–574.
44 H. Sehaqui, A. Liu, Q. Zhou and L. A. Berglund, *Biomacromolecules*, 2010, **11**, 2195–2198.
45 J. Sugiyama, R. Vuong and H. Chanzy, *Macromolecules*, 1991, **24**, 4168–4175.